Structural and magnetic phase transitions in Mn-Ni alloys

R. S. Fishman and W.-T. Lee
Solid State Division, Oak Ridge National Laboratory, Oak Ridge, Tennessee 37831-6032

S. H. Liu
Department of Physics, University of California, San Diego, California 92093

D. Mandrus and J. L. Robertson
Solid State Division, Oak Ridge National Laboratory, Oak Ridge, Tennessee 37831-6032

K. J. Song and J. R. Thompson
Solid State Division, Oak Ridge National Laboratory, Oak Ridge, Tennessee 37831-6032
and University of Tennessee, Knoxville, Tennessee 37996-1200
(Received 5 August 1999; revised manuscript received 6 January 2000)

When the Ni concentration exceeds about 18%, Mn-Ni alloys were expected to support two different noncollinear spin-density wave (SDW) phases. A triple-Q SDW with moments along the crystal diagonals was believed to appear in the fcc phase between T_N and T_t. Below T_t, the fct phase with $c>a$ was believed to contain a double-Q SDW with moments in the ab plane and at 45° angles from the crystal axes. Based on resistivity, neutron-scattering, and susceptibility measurements, we show that the structural and magnetic phase transitions in a $Mn_{1-x}Ni_x$ alloy with $x\approx 0.20$ are actually distinct, with the structural phase transition at $T_t \approx 250$ K lying far above the magnetic transition at $T_m \approx 125$ K. A Hamiltonian which includes elastic, magnetoelastic, and noncollinearity energies is used to describe these two transitions. In the tetragonal phase between T_t and T_m, our model predicts a new SDW phase with moments tilted away from the crystal diagonals toward the ab plane. The energy gap in the spin-wave spectrum is predicted to change discontinuously at T_m.

I. INTRODUCTION

The recent observation of a helical spin-density wave (SDW) in Fe/Cr multilayers[1] has renewed interest in the stability of noncollinear SDW's[2] in bulk transition metals. In all likelihood, γ-Mn alloys are the simplest bulk metals to support noncollinear SDW's. Because the fcc phase of pure Mn is only stable at high temperatures, γ-Mn is produced by doping[3] with a few percent of Ni, Cu, or Fe. Due to strong magnetoelastic energies,[4–7] the Néel temperature T_N coincides with a cubic-to-tetragonal distortion[8–11] in lightly doped γ-Mn alloys. Phenomenological models[4,7] suggest that the experimental phase diagram of Mn-Ni alloys[11] reproduced in Fig. 1 contains two noncollinear or multiple (M) SDW's. When the Ni concentration exceeds about 18%, a triple-Q SDW with moments along the crystal diagonals was predicted in the cubic phase between T_N and T_t. Below T_t, the crystal becomes tetragonal with $c/a>1$. Assuming that this structural phase transition is also driven by magnetoelastic energies, then the SDW below T_t was predicted to have a double-Q structure with the spins lying in the ab plane and pointing at 45° angles to the crystal axis. Along with the collinear, single-Q SDW expected in the tetragonal phase of lightly doped alloys with $c/a<1$, these two M SDW configurations are sketched in Fig. 2(a).

We provide experimental evidence that this picture is wrong. Studies of a Mn-Ni polycrystal with a Ni concentration of 20% and a Néel temperature of about 450 K reveal that the magnetic transition between different SDW phases at $T_m \approx 125$ K lies far below the cubic-to-tetragonal structural transition at $T_t \approx 250$ K. As first shown almost thirty years ago,[10,11] the cubic-to-tetragonal transition in Mn-Ni alloys is easy to observe using x rays or neutrons. But it has proven very difficult to distinguish one SDW phase from another. Even the presence of noncollinear SDW states in γ-Mn alloys has been in doubt.[12]

The usual tool to identify SDW phases is elastic neutron

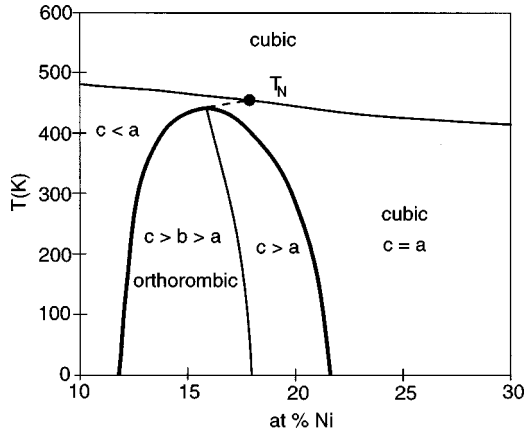

FIG. 1. The structural phase diagram of $Mn_{1-x}Ni_x$ alloys taken from Ref. 11. As discussed in Sec. IV, the thick curve is believed to coincide with the condition $A(T)=A_c$ or $c_{11}^0-c_{12}^0+A(T)=0$. The dashed line from T_t to the triple point (denoted by the filled circle) is the conjectured phase boundary between the S and T SDW phases, as discussed in the text.

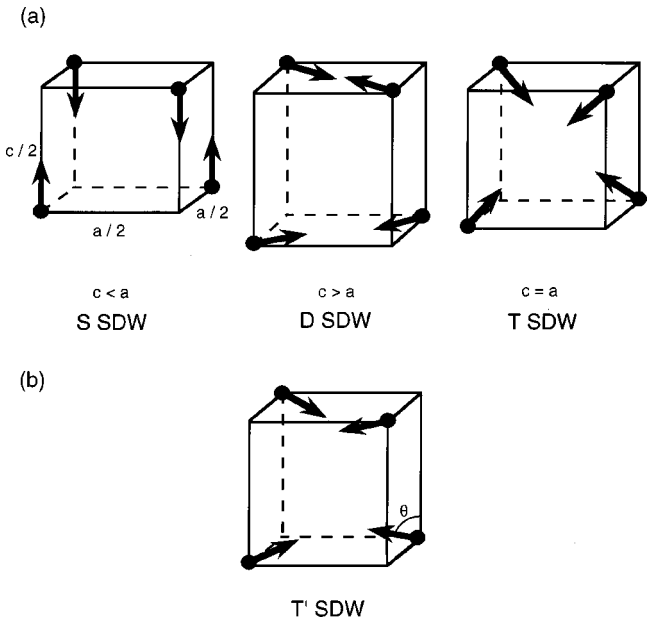

FIG. 2. (a) The *S*, *D*, and *T* SDW phases which are stabilized in different crystal structures. (b) The proposed T' SDW phase between T_t and T_m.

scattering. But in γ-Mn alloys, neutrons are unable to separately distinguish the SDW phases in Fig. 2(a) due to the contribution of different domains.[8,13] If only a single SDW domain was present, the SDW phases would be easy to tell apart: while all magnetic satellites would appear for the *T* SDW structure, only 1/2 of those satellites would be active for the *D* SDW structure, and only 1/3 would be active in the *S* SDW structure. But after averaging over the three possible domains of the *S* and *D* SDW phases, the elastic scattering from each magnetic state becomes identical.

As alternatives to neutron-scattering, Mössbauer transmission,[14] and γ-ray emission[15] measurements have been tried. Both techniques suggested the presence of *M* SDW phases in Mn-Ni and Fe-Mn alloys. However, it would be cumbersome to use such atomic-scale probes to map the SDW phase as a function of doping and temperature.

Very recently, two of us (R.F. and S.L.) demonstrated[16] that the magnetic susceptibility of the three SDW configurations in Fig. 2(a) are slightly different, even after averaging over possible SDW domains. Consequently, the transition from one SDW configuration to another will be marked by a small jump in the susceptibility. Depending on the relative sizes of the electron and hole Fermi surfaces, which nest to produce the SDW order in γ-Mn alloys,[17] the susceptibility can jump up or down. The magnetic susceptibility may be the only bulk probe able to easily distinguish one SDW phase from another in the presence of multiple domains.[18]

Susceptibility measurements on the Mn-Ni sample described above detected a magnetic transition at about 125 K. The susceptibilty of the low-temperature phase is about 3.5% smaller than that of the high-temperature phase. No significant change in the susceptibility was observed at the structural phase-transition temperature of 250 K.

To explain the distinct structural and magnetic transitions, we construct a phenomenological model which includes both elastic and magnetoelastic contributions. The noncollinear, *M* SDW states are stabilized by a noncollinearity energy $E_{\rm NC}$, which is produced by the difference between the Mn and Ni moments.[19,20] We have constructed $E_{\rm NC}$ to favor the *T* SDW phase over the *D* SDW phase and the *D* SDW phase over the *S* SDW phase.

Our model assumes that the softening of $c_{11}-c_{12}$ breaks the cubic symmetry below T_t. So the transition at T_t is not driven by magnetoelastic interactions. Rather, the magnetic structure below T_t responds to the tetragonal distortion by tilting towards the ab plane. When the tetragonality becomes sufficiently large, the SDW transforms from a ''tilted'' *T* SDW (or T' SDW) state to a *D* SDW state.

Just below T_N, this model predicts the formation of either a *S* SDW state for small Ni concentrations or a *T* SDW state for larger Ni concentrations. In agreement with experiments, we conclude that the *D* SDW phase is never stable just below the Néel transition. In fact, the *D* SDW phase must be preceeded at a higher temperature by a structural phase transition into a tetragonal state with $c>a$.

This paper is divided into four sections. Section II contains our experimental results for the structural and magnetic phase transitions. In Sec. III, we present a simple model which describes the distinct structural and magnetic phase transitions. Finally, Sec. IV contains a discussion and conclusion. An appendix contains some results for the elastic constants of our model Hamiltonian.

II. STRUCTURAL AND MAGNETIC PHASE TRANSITIONS

The Mn-Ni samples were prepared by arc melting in an argon atmosphere from Mn (99.98%) and Ni (99.99%) pieces obtained from Johnson Matthey. Each ingot was flipped and remelted several times to promote homogeneity. A starting composition of $Mn_{0.81}Ni_{0.19}$ produced a final composition of $Mn_{0.80}Ni_{0.20}$ due to volatilization of Mn. After arc melting, the samples were sealed under vacuum in silica tubes, annealed for 2 days at 950°C, and then quenched to room temperature.

A. Resistivity

Resistivity measurements were performed using a conventional linear four-probe method. Contacts to the sample were made using Cu wires and Epotek H20-E silver epoxy. As shown in Fig. 3, the resisitivity above 250 K is fit rather well by a linear temperature dependence. Deviation from this linear fit occurs below 250 K, with the resistivity initially dropping below the linear fit and then passing above it at 110 K. As confirmed in the next subsection, the deviation of the resistivity from linearity marks the cubic-to-tetragonal at $T_t \approx 250$ K. There is no obvious signature in the resistivity of the magnetic phase transition at $T_m \approx 125$ K.

B. Neutron-scattering results

A 2.1 g sample of $Mn_{0.80}Ni_{0.20}$ was studied in an elastic neutron scattering experiment[21] performed on the HB1 triple-axis spectrometer at the High Flux Isotope Reactor of Oak Ridge National Laboratory. Data was collected between 50 and 275 K. Although we did not heat the sample to detect the Néel transition, previous work[11] suggests that $T_N \approx 450$ K.

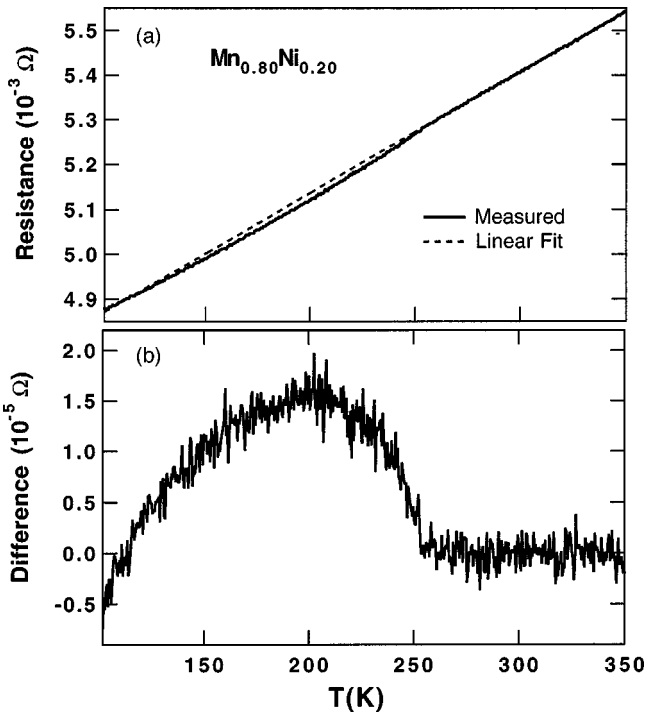

FIG. 3. (a) The resitivity of Mn-Ni versus temperature. The dashed line is a linear fit to the resistivity above 250 K. (b) The difference between the resistivity and the linear fit showing the resistivity anomaly at 250 K.

As the sample was rotated, we observed a small variation in the Bragg peak intensity due to the texture of the sample. Subsequently, we repeated the measurements at 2° step increments of the sample angle. At each temperature, ten such data sets were averaged to eliminate the texture effects.

In Figs. 4(a) and 4(b), we plot the scattering intensity profiles at 275 and 225 K as a function of the momentum transfer Q near the {200} reflections. The peaks were broadened by the finite resolution of the spectrometer[22] $\delta Q = 0.04$ Å^{-1} and the peak profiles were approximated by Gaussians, which are drawn as solid curves. Only a single

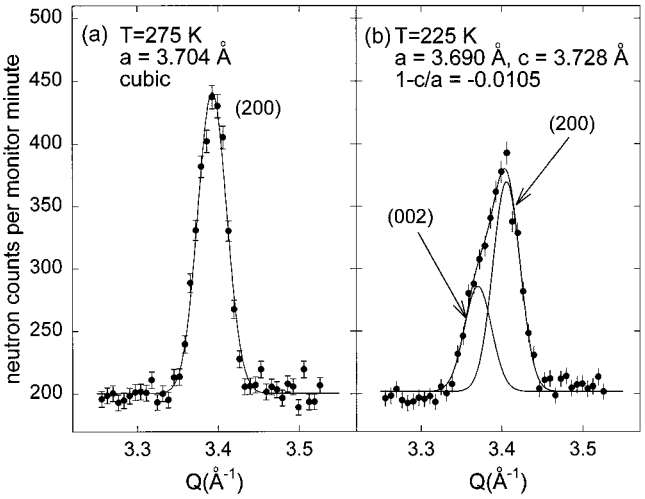

FIG. 4. Neutron-scattering intensity profiles as a function of the momentum transfer Q for (a) 275 K and (b) 225 K. The scans were taken at the {200} Bragg points.

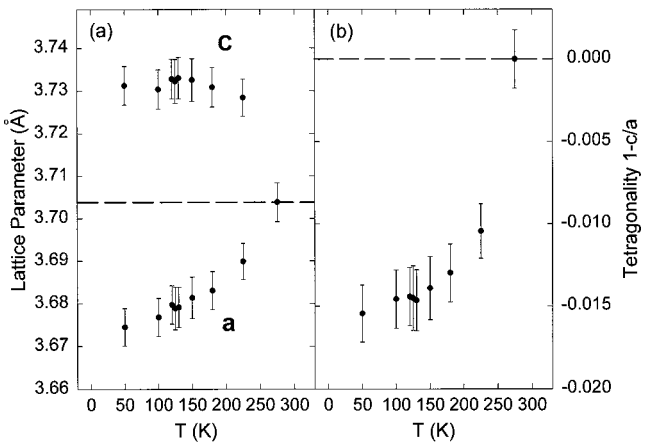

FIG. 5. (a) Lattice parameters a and c versus temperature, showing a cubic-to-tetragonal phase transition between 275 and 225 K. (b) The tetragonality $t = 1 - c/a$ versus temperature.

Gaussian was required to fit the data at 275 K, which indicates that the reflections from the (200), (020), and (002) lattice planes overlapped. The crystal structure at 275 K was cubic with the lattice parameter $a = c = 3.704$ Å. By contrast, a double Gaussian was required to fit the intensity profile at 225 K. The peak height at the lower scattering angle is about half of the peak height at the higher scattering angle, which is expected for a tetragonal distortion. Since the lower peak was shifted downwards compared to the cubic structure while the higher peak was shifted upwards, we conclude that $c > a$ in the tetragonal phase. Based on the fit at 225 K, we obtain the lattice parameters $c = 3.728$ Å and $a = 3.690$ Å. The integrated intensity of the profile at 275 K is identical, within experimental error, to that at 225 K. These results are all consistent with a cubic-to-tetragonal phase transition.

The lattice parameters are plotted as a function of temperature in Fig. 5(a). Clearly, the structural phase transition occurs between 275 and 225 K. As the temperature decreases further, the neighboring basal plane distance c increases while the basal planes continue to contract. Using the measured lattice parameters, we find that the unit cell volume decreases almost linearly with decreasing temperature. The tetragonality $t = 1 - c/a$ is plotted in Fig. 5(b). Extrapolating t to zero temperature yields a value of c/a between 1.016 and 1.017. Our results are consistent with measurements made by Uchishiba[10] and Honda *et al.*[11] who obtained low-temperature c/a ratios of 1.011 and 1.014, respectively, on Mn-Ni alloys of similar composition. While our data is not good enough to distinguish the order of the structural phase transition, the work of Uchishiba and Honda *et al.* suggests that it is second order.

C. Susceptibility measurements

Magnetic studies of the Mn-Ni alloy were conducted in a SQUID-based magnetometer (Quantum Design model MPMS-7). A 0.9377 g sample was cut from the same ingot as the resistivity and neutron-scattering samples. This sample was mounted with thread in a thin-wall plastic tube for measurements with a scan length of 4 cm. The isothermal magnetization was measured at several temperatures between 5

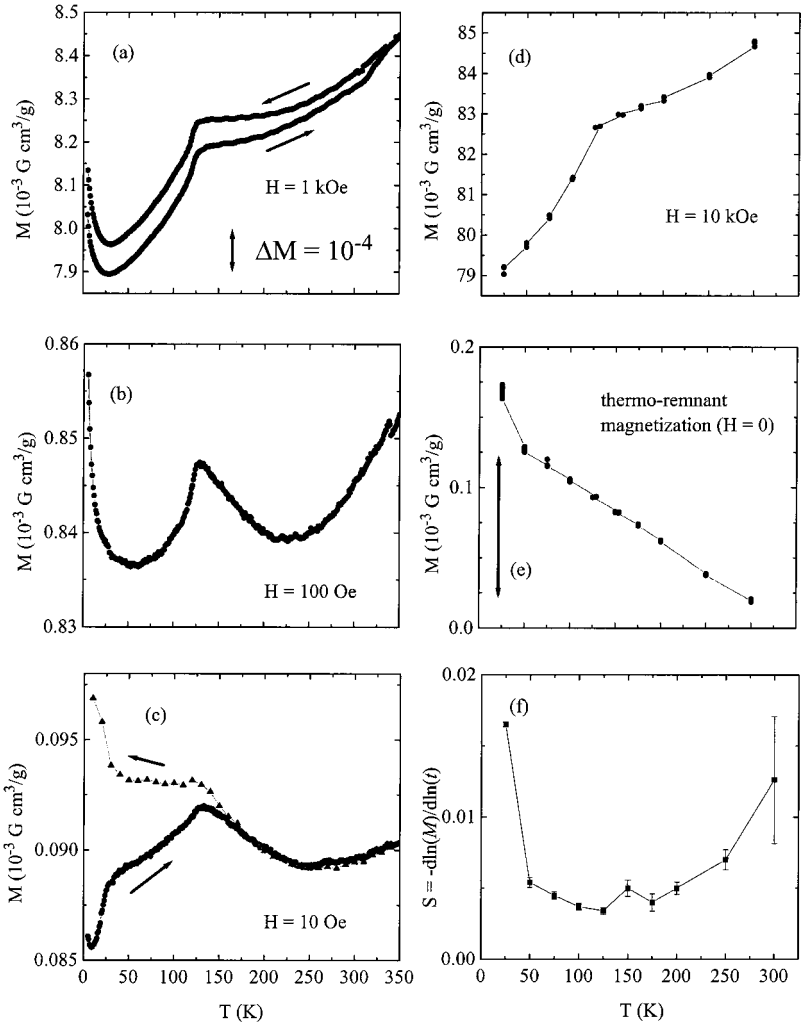

FIG. 6. Magnetization for fields of (a) 1000 G, (b) 100 G, and (c) 10 G with arrows indicating whether the data was taken during cooling or heating. The field-cooled magnetization for 10 kG is shown in (d). After this field is removed, we obtain the remnant magnetization in (e) and the normalized relaxation rate S in (f), as described in the text.

and 300 K, in applied magnetic fields H up to 65 kG. Overall, the magnetic response was very nearly linear and reversible at all temperatures.

The temperature dependence of the magnetization M was obtained by cooling the sample in zero field to 5 K, at which point the field was applied and trapped in the superconducting solenoid. Then the magnetic moment was measured on a fine grid of temperatures while warming to 360 K; subsequent field-cooled measurements were conducted while recooling to 5 K.

Results of these magnetic studies are shown in Figs. 6(a)-6(c) for fields of 1000, 100, and 10 G. The most striking feature is the structure near 125 K, which lies far below the structural transition at 250 K. The sharp drop in the susceptibility at 125 K is of the same order predicted by Fishman and Liu[16] and may be ascribed to a magnetic phase transition between two different SDW phases. The only magnetic feature obviously correlated with the cubic-to-tetragonal transition is a broad, very shallow minimum in the magnetization.

The hysteretic behavior seen in Fig. 6(c) for a field of 10 G is somewhat reminiscent of the spin-glass transition observed in MnCu alloys.[23] To further characterize this behavior, we performed a series of magnetic relaxation measurements. After applying a field of 10 kG at 300 K, the MnNi sample was field-cooled to temperature T with magnetization $M(T)$ plotted in Fig. 6(d). The field was subsequently removed and the magnet in the SQUID magnetometer was ''reset'' (heated above the superconducting transition temperature of the windings) to release any trapped field. Finally, the remnant magnetization $M(t)$ plotted in Fig. 6(e) was measured as a function of time t for a period of one hour. The time dependence of $M(t)$ was used to obtain the normalized relaxation rate (the magnetic viscosity) $S = -d\ln(M)/d\ln(t)$, which is plotted in Fig. 6(f).

All of these measurements indicate that the susceptibility anomaly at 125 K is not associated with the hysteretic behavior of the sample at low fields. From Fig. 6(d), we find that the field-cooled magnetization in the 10 kG field is large and exhibits the same transition at 125 K as observed in lower fields. If produced by a spin-glass transition, the anomaly would be suppressed at higher fields.[24] As shown in Fig. 6(e), the remnant magnetization $M_{\rm rem}$ is small compared with the signal observed in $H=1$ and 10 kG. The vertical arrows in frames (a) and (e) of Fig. 6 show identical changes in M of 10^{-4} G cm^3/g; in frame (d), this range is smaller than the symbol size. Also notice that the remnant magnetization $M_{\rm rem}$ is featureless below 300 K. In Fig. 6(f), we find that the magnetic relaxation rate $S(T)$ is also small and featureless in the region of the SDW transition near 125 K. To illustrate that the change in $M_{\rm rem}$ during the hour of measurement is small, all measured values are collected in Fig. 6(e). Finally, analysis of the isothermal magnetization, $M(H) = \chi_l H + \chi_{\rm nl} H^3$, reveals that the nonlinear term $\chi_{\rm nl}$ vanishes

(within two standard deviations). In contrast to the expectation for a spin-glass transition,[25] no change in χ_{nl} was observed near 125 K.

Because there is no sudden onset of large-scale glassy behavior (time-dependent or nonlinear effects) at 125 K, we conclude that the susceptibility anomaly is not associated with a spin-glass transition. The weak glassiness observed in a 10 G field may be attributed to the freezing of the Ni moments in a disordered alloy. But we emphasize that these effects are small compared with the SDW transition at 125 K.

At low temperatures below 40 K there is an upturn in the magnetization that follows a Curie $1/T$ dependence. The observed signal corresponds to an effective moment of 0.023μB per atom. We have verified that this feature is more pronounced in dirty samples and so is likely caused by contamination of the sample surface.

III. MODEL FOR THE STRUCTURAL AND MAGNETIC TRANSITIONS

In the next three subsections, we present a model for the separate structural and magnetic phase transitions observed in Mn-Ni. First, we construct a model Hamiltonian, then we discuss the SDW ordering between T_N and the structural transition at T_t, and finally, we describe the SDW ordering below T_t.

A. Model Hamiltonian

In addition to the three magnetic phases previously proposed for cubic and tetragonal Mn-Ni alloys, we also consider a fourth SDW phase which interpolates between them. The average spins $\mathbf{M}_i=\langle \mathbf{S}_i\rangle$ of the *S*, *D*, *T*, and tilted *T* (or T') SDW spin structures may be written as

$$\mathbf{M}_i = M\hat{z}\cos(\mathbf{Q}_z\cdot\mathbf{R}_i), \tag{1a}$$

$$\mathbf{M}_i = \frac{1}{\sqrt{2}}M[\hat{x}\cos(\mathbf{Q}_x\cdot\mathbf{R}_i)+\hat{y}\cos(\mathbf{Q}_y\cdot\mathbf{R}_i)], \tag{1b}$$

$$\mathbf{M}_i = \frac{1}{\sqrt{3}}M[\hat{x}\cos(\mathbf{Q}_x\cdot\mathbf{R}_i)+\hat{y}\cos(\mathbf{Q}_y\cdot\mathbf{R}_i)+\hat{z}\cos(\mathbf{Q}_z\cdot\mathbf{R}_i)], \tag{1c}$$

$$\mathbf{M}_i = \frac{1}{\sqrt{3}}M\{\sqrt{1+\nu/2}[\hat{x}\cos(\mathbf{Q}_x\cdot\mathbf{R}_i)+\hat{y}\cos(\mathbf{Q}_y\cdot\mathbf{R}_i)] + \sqrt{1-\nu}\,\hat{z}\cos(\mathbf{Q}_z\cdot\mathbf{R}_i)\}, \tag{1d}$$

where $\mathbf{Q}_x=2\pi\hat{x}/a$, $\mathbf{Q}_y=2\pi\hat{y}/a$, $\mathbf{Q}_z=2\pi\hat{z}/c$, and $\cos(\mathbf{Q}_\gamma\cdot\mathbf{R}_i)=\pm 1$. These relations are obtained by replacing the sharply peaked Bloch wave functions of the *d*-band electrons by delta functions in the spin density. While the *T* SDW phase of Eq. (1c) maintains cubic symmetry, the T' SDW phase of Eq. (1d) with $\nu\neq 0$ violates it. Note that the T' SDW phase reduces to the *T* SDW phase when $\nu=0$, to the *S* SDW phase when $\nu=-2$, and to the *D* SDW phase when $\nu=1$.

Our model Hamiltonian contains five different terms

$$H = H_0 + H_{\mathrm{Coul}} + H_{\mathrm{el}} + H_{\mathrm{me}} + H_{\mathrm{NC}}, \tag{2}$$

where H_0 is the kinetic energy of the electrons and holes and H_{Coul} is the Coulomb attraction between the electrons and holes on nearly nested Fermi surfaces.[7] Although essential to obtain the magnetization $M(T)$, H_0 and H_{Coul} play no role in selecting the phase of the SDW. So we shall not discuss them further. The other three energies are explicitly given by

$$H_{el} = V\left\{\frac{1}{2}c_{11}^0(\epsilon_{xx}^2+\epsilon_{yy}^2+\epsilon_{zz}^2)+c_{12}^0(\epsilon_{xx}\epsilon_{yy}+\epsilon_{yy}\epsilon_{zz}+\epsilon_{zz}\epsilon_{xx}) + \frac{2}{9}A(t_x^2+t_y^2+t_z^2)+U(t_x^2+t_y^2+t_z^2)^2+W(t_x^4+t_y^4+t_z^4)\right\}, \tag{3}$$

$$H_{\mathrm{me}} = V\left\{\frac{g_1}{N}\sum_i (S_{ix}^2\epsilon_{xx}+S_{iy}^2\epsilon_{yy}+S_{iz}^2\epsilon_{zz})+(\epsilon_{xx}+\epsilon_{yy}+\epsilon_{zz}) \times\left[\frac{g_2}{N}\sum_i (S_{ix}^2+S_{iy}^2+S_{iz}^2) + \frac{g_3}{N}\sum_i (S_{ix}^4+S_{iy}^4+S_{iz}^4)\right]\right\}, \tag{4}$$

$$H_{\mathrm{NC}} = V\xi\left\{\frac{1}{N}\sum_i (S_{ix}^2+S_{iy}^2-2S_{iz}^2)\right\}^2, \tag{5}$$

where $t_x=(\epsilon_{yy}+\epsilon_{zz})/2-\epsilon_{xx}$, $t_y=(\epsilon_{zz}+\epsilon_{xx})/2-\epsilon_{yy}$, and $t_z=(\epsilon_{xx}+\epsilon_{yy})/2-\epsilon_{zz}$ are the tetragonalities, ϵ_{ii} are the strain components, c_{11}^0 and c_{12}^0 are elastic constants, and g_i are the magnetoelastic coupling strengths. We assume that c_{11}^0 and c_{12}^0 are independent of temperature so that the structural phase transition is driven by the temperature dependence of $A(T)$.

Above T_t, cubic symmetry requires that $t_x=t_y=t_z$. Below T_t, cubic symmetry is broken with $t_x=t_y=-t_z/2 \equiv -t/2$. The quartic t_z^4 coefficient is then given by $B=9(U+W/2)$, which must be positive for the structural phase transition to be second order. The total elastic constants c_{ij} of the cubic and tetragonal phases are summarized in the Appendix along with the stability criterion for those phases. In particular, we find that stability of the cubic structure requires $c_{11}-c_{12}=c_{11}^0-c_{12}^0+A$ to be positive.

For convenience, we have neglected off-diagonal strain components such as ϵ_{yz}. Off-diagonal strain components are much smaller than the diagonal components if the elastic constant c_{44} is much larger than the constants c_{11} and c_{12} of the cubic structure. Since c_{44} is not involved in the tetragonal instability in Mn-Ni and Fe-Mn alloys, this approximation is justified.

Our model for the tetragonal transition takes strain as the primary order parameter. In an alternative formulation,[26] a soft mode would act as the primary order parameter driving the structural phase transition. Playing the role of secondary order parameter, strain would then couple to the square of the primary order parameter. There are several reasons for our decision to use strain as the primary order parameter. First, the theory is a bit simpler this way. Second, experiments by Lowde *et al.*[27] indicate that the softening of c_{11}

$-c_{12}$ preceeds the tetragonal transition. Third, it is not clear what soft mode would drive the tetragonal transition in γ-Mn alloys. In any case, a model built upon a soft mode produces the same qualitative conclusions as the model developed below.

Physically, the noncollinearity energy arises from the difference between the Mn and impurity moments, which causes the Mn moments to tilt away from each other.[19,20] This effect is most pronounced in Mn-Cu alloys, where the Cu atoms carry no moment and even in the S SDW phase, the Mn moments are inclined about 5° from the z axis.[28] The noncollinearity energy in Eq. (5) yields the expectation value $V\xi\nu^2M^4$. In terms of the average spin $\mathbf{M}_i$ or the angle θ defined in Fig. 2(b), the ''tilt'' is given by $\nu=(M_{ix}^2+M_{iy}^2-2M_{iz}^2)/M^2=1-3\cos^2\theta$. Therefore, ν can be viewed as the magnetic tetragonality. In the absence of magnetoelastic energies, deviations from the T SDW state with $|\nu|<1$ have the same energy regardless of whether the moments tilt toward the ab plane ($\nu>0$) or towards the c axis ($\nu<0$).

Both the noncollinearity and quartic g_3 energies act to stabilize a T' SDW state with $\nu\neq 0$ in the tetragonally distorted lattice between T_t and T_m. To see this, replace the magnetoelastic and noncollinearity energies with the effective Hamiltonian

$$H'_{\rm men}=-\sum_i \mathbf{B}_i\cdot\mathbf{S}_i+\text{const}, \tag{6}$$

$$B_{i\gamma}=-2\frac{V}{N}\{g_1\epsilon_{\gamma\gamma}+(g_2+2g_3M_{i\gamma}^2)(\epsilon_{xx}+\epsilon_{yy}+\epsilon_{zz}) +(2-6\delta_{\gamma z})\nu\xi M^2\}M_{i\gamma}. \tag{7}$$

Within this mean-field approximation, every electron and hole independently experiences the effective field $\mathbf{B}_i$ exerted by the magnetoelastic and noncollinearity energies. For each magnetic phase, stability requires that $\mathbf{B}_i$ is parallel to $\mathbf{M}_i$. Without the noncollinearity and quartic terms, only the S or D SDW phases could be stable in a tetragonally distorted crystal. But with ξ and g_3 nonzero, the T' SDW phase is stabilized with tilt

$$\nu=-\frac{g_1 t}{(g_3 s+6\xi)M^2}, \tag{8}$$

where $s\equiv\Delta V/V=\epsilon_{xx}+\epsilon_{yy}+\epsilon_{zz}=2\epsilon_{xx}+\epsilon_{zz}$ is the fractional volume change below T_N.

We shall see that the g_3 term is also important for determining the order of the magnetic transition at T_m. When $g_3=0$, the transition is second order with the tilt of the T' SDW matching the tilt of the D SDW at T_m. When $g_3\neq 0$, the transition is first order with the tilt of the SDW changing discontinously at T_m. We realize that the g_3 contribution in Eq. (4) is not the only quartic energy consistent with cubic symmetry which can produce a first-order transition. For example, the quartic term $g_4\Sigma_i(\epsilon_{xx}S_{ix}^4+\epsilon_{yy}S_{iy}^4+\epsilon_{zz}S_{iz}^4)$ also does the trick. However, other quartic terms have qualitatively the same effect as the g_3 term and would needlessly complicate our model. So to keep the theory as simple as possible, we shall retain only the single g_3 quartic term.

Minimizing the Hamiltonian with respect to the strain components, we find that the relative volume change below T_N is

$$s=-\frac{g_1+3g_2+g_3M^2(1+\nu^2/2)}{c_{11}^0+2c_{12}^0}M^2 \tag{9}$$

and that the tetragonality t is obtained from the cubic equation

$$t^3+\frac{2(A-A_c)}{3B}t+M^2\frac{g_1}{3B}\nu=0, \tag{10}$$

where $A_c\equiv c_{12}^0-c_{11}^0$. For $A>A_c$,[29] the crystal remains cubic with $t=0$ and $\nu=0$. For $A<A_c$, the crystal becomes tetragonal with $t\neq 0$. Above T_t, Eqs. (A2) and (A3) imply that $A-A_c=c_{11}-c_{12}$. Hence, the vanishing of $A-A_c$ corresponds to the softening of $c_{11}-c_{12}$, which has been observed[27] to preceed the tetragonal transition in a series of Mn-Ni-C alloys. Notice that this tetragonal instability is not driven by the magnetoelastic energies. Close to T_t, $c_{11}-c_{12}$ is a linear function of temperature[27] and $A-A_c$ can be replaced by $\alpha(T-T_t)$ with $\alpha>0$.

In terms of the volume expansion and tetragonality, the combined magnetoelastic and noncollinearity energy of the S, D, and T SDW states is given by

$$\frac{E_{\rm men}}{V}=-\frac{1}{6}s^2(c_{11}^0+2c_{12}^0)+\frac{1}{3}t\left\{(c_{11}^0-c_{12}^0+A)t+M^2g_1\nu+\frac{3}{4}Bt^3\right\}+\xi\nu^2M^4, \tag{11}$$

which does not include the kinetic and Coulomb terms. Not surprisingly, minimizing $E_{\rm men}$ with respect to t for fixed ν yields Eq. (10). For a fixed t, the condition $\partial E_{\rm men}/\partial\nu=0$ yields Eq. (8), which was obtained above from the condition that the effective field $\mathbf{B}_i$ is parallel to $\mathbf{M}_i$. Bear in mind, however, that Eq. (8) may produce a maximum in $E_{\rm men}$, in which case S and D SDW's with $\nu=-2$ and 1 will have lower energies.

The magnetoelastic constants g_1 and g_2 are assumed to be of the same order with respect to each other but rather small compared to the elastic constants except very close to T_t. Since the observed volume contraction in Mn-Ni is about 1%, we expect that $(g_1+3g_2)/c_{11}\sim 0.01$. It is likely that the quartic coefficient g_3 is an order-of-magnitude smaller than the quadratic coefficients g_1 and g_2.

Not too close to T_t, the approximation

$$|A(T)-A_c|^3\gg Bg_1^2M^4 \tag{12}$$

or $|T-T_t|^3\gg Bg_1^2M^4/\alpha^3$ should hold rather well. This condition will be used to solve for the tetragonality in the two subsections below.

B. SDW ordering between T_N and T_t

Applying Eq. (12) when $A(T)>A_c$ or $T>T_t$, the tetragonality below T_N is given by

$$t(T)\approx -M(T)^2\nu\frac{g_1}{2}\frac{1}{A(T)-A_c}, \tag{13}$$

with a next-order term of order $g_1^3M(T)^6B/[A(T)-A_c]^4$. Substituting this value into Eq. (11), we obtain the energy of a general T' SDW state

$$\frac{E_{\rm men}}{V}=-\frac{1}{6}M^4\frac{[g_1+3g_2+g_3M^2(1+\nu^2/2)]^2}{c_{11}^0+2c_{12}^0} -\left\{\frac{g_1^2}{12}\frac{1}{A-A_c}-\xi\right\}\nu^2M^4. \tag{14}$$

Close to T_N, the $(g_1+3g_2)g_3(1+\nu^2/2)M^6$ term can be neglected compared to the ν^2M^4 term. Then the SDW phase must minimize the ν^2M^4 term in Eq. (14).

Recall that the noncollinearity parameter ξ is expected to increase with the Ni or Fe concentration. When $\xi=0$, the ν^2M^4 term is negative and the S SDW (with $\nu=-2$) has the lowest energy close to T_N. The T SDW (with $\nu=0$) is favored over the S SDW when the ν^2M^4 term becomes positive or when ξ exceeds

$$\xi_0=\frac{g_1^2}{12}\frac{1}{A(T_N)-A_c}. \tag{15}$$

Consulting the phase diagram in Fig. 1, we see that T_t approaches quite close to T_N at the top of the cubic-to-tetragonal phase boundary. So ξ_0 will be quite large for $x\approx 16\%$. Therefore, the T SDW phase is only stabilized for higher values of x, when T_t drops sufficiently far below T_N that $\xi_0<\xi$. For this reason, we construct the dashed phase boundary (not yet fixed by any experimental data) between the S and T SDW states to approach the triple point from the left. The stability of the T SDW phase against tilting above T_t is guaranteed by the condition $\partial^2E_{\rm men}/\partial\nu^2|_{\nu=0}>0$, which requires that $g_3s+6\xi>0$.

If $A(T)>A_c$ for all temperatures, then the energetics of the SDW configurations would be determined by Eq. (14), including terms of order M^6 and M^8. The transition from a T to a S SDW, as in Fe-Mn alloys,[9] can be easily described by this model. When $A(T)>A_c$ for all temperatures, the structural phase transition at T_t is induced by magnetoelastic energies and $T_m=T_t$. Since each term in Eq. (14) favors either the S or T SDW phase, the D SDW phase is unstable when $A(T)>A_c$. It follows that, whereas Fe-Mn alloys can be completely described by Eq. (14), Mn-Ni alloys require a tetragonal instability, induced by the softening of $A(T)-A_c=c_{11}-c_{12}$, to accommodate the D SDW phase. We shall return to this point in Sec. IV.

C. SDW ordering below T_t

As shown in the appendix, the stability of the tetragonal phase below T_t requires that $A(T)<A_c$. Using Eqs. (10) and (12), we obtain the tetragonality

$$t(T)\approx\pm\sqrt{\frac{2[A_c-A(T)]}{3B}}-\frac{1}{4}M(T)^2g_1\nu(T)\frac{1}{A_c-A(T)}, \tag{16}$$

where the first term dominates the second due to Eq. (12). Although the overall sign of t below T_t is not determined by this model, we expect material parameters to break the symmetry between positive and negative tetragonalities.

Inserting this expression into Eq. (11), we find that the energy of a general T' SDW is given by

$$\frac{E_{\rm men}}{V}=-\frac{1}{6}M^4\frac{[g_1+3g_2+g_3M^2(1+\nu^2/2)]^2}{c_{11}^0+2c_{12}^0}-\frac{(A_c-A)^2}{9B} +\frac{\sqrt{6}}{9}M^2g_1\nu\sqrt{\frac{A_c-A}{B}}\ \mathrm{sgn}(t)+\xi\nu^2M^4. \tag{17}$$

This energy favors a negative value of $g_1\nu\ \mathrm{sgn}(t)$ so that the preferred tilt of the T' SDW phase depends on the sign of the tetragonality. Since the S and D SDW phases are stable in crystals with $t>0$ and $t<0$, respectively, g_1 must be positive.

For a tetragonal phase with $t>0$, such as in Fe-Mn alloys, the T' SDW would tilt towards the c axis and transform into a S SDW below T_t. But as argued in the next section, the structural and magnetic transitions must coincide in Fe-Mn alloys. Hence, the theory developed in this subsection with $A(T)<A_c$ applies only to Mn-Ni alloys.

Within the tetragonal phase of Mn-Ni alloys with $t<0$, the T' SDW transforms into a D SDW below T_m, which is given to lowest order in g_i by

$$\frac{A_c-A(T_m)}{B}=\frac{27\xi^2M(T_m)^4}{2g_1^2}[1+\nu(T_m^+)]^2, \tag{18}$$

Together with Eq. (12), this relation implies that $g_1^4\ll\xi^3M^4B$. Notice that $A_c-A(T_m)=\alpha(T_t-T_m)$ grows with increasing impurity concentration (increasing ξ) and with decreasing T_m (increasing M).

Between T_t and T_m, the moments of the T' SDW state tilt towards the ab plane. Just above T_m, the tilt is given by

$$\nu(T_m^+)=\frac{3\xi}{g_3s+3\xi}. \tag{19}$$

The inequality $\nu\leqslant 1$ requires that $g_3s\geqslant 0$, which also guarantees the stability of the T SDW phase. Due to the observed volume compression[11] below T_N, we conclude that $g_3\leqslant 0$. If $g_3=0$, then the transition at T_m would be second order and the tilt of the T' SDW just above T_m would exactly match the tilt $\nu=1$ of the D SDW below T_m. Of course, the observed jump in the magnetic susceptibility at T_m implies that g_3 is nonzero in Mn-Ni alloys. So we expect the tilt of the T' SDW just above the first-order transition at T_m to be smaller than the tilt of the D SDW below T_m.

For $g_3<0$, this model predicts a small change in the tetragonality at T_m. But Eqs. (16), (18), and (19) may be used to show that the relative change in t at T_m is given by

$$\frac{t^{T'}-t^D}{t^{T'}}=-\frac{g_1^4g_3s}{162BM(T_m)^4\xi^3}\frac{(g_3s+3\xi)^2}{(g_3s+6\xi)^3}<0, \tag{20}$$

which is very small for $g_1^4 \ll \xi^3 M^4 B$. The measurements of Honda *et al.*[11] and the neutron-scattering results of Fig. 5(b) suggest that the drop in t below T_m is too small to be measured.

As discussed in previous work,[7] the formation of a SDW in a fcc crystal differs from its formation in a bcc crystal because only 1/3 of the holes are paired to electrons in the electron-hole condensate. While the holes in the condensate experience an energy gap $\Delta(T) \propto M(T)$, the remaining holes are unaffected by the formation of the SDW. Although the quasiparticle energies are redistributed at T_m, the number of holes which experience an energy gap remains the same on both sides of the transition. Consequently, the energy gap itself is unaffected by the magnetic transition and the resistivity is not expected to show any signature of a phase transition between different magnetic configurations with the same crystal structure. Of course, this is consistent with the resistivity measurements presented in Sec. IIA.

IV. DISCUSSION AND CONCLUSION

In this paper, we have shown that the magnetic and structural phase transitions in a Mn-Ni alloy occur at different temperatures. The structural phase transition from cubic to tetragonal at $T_t \approx 250$ K was determined using resistivity and neutron-scattering measurements; the magnetic transition at $T_m \approx 125$ K was detected in the magnetic susceptibility. While the tetragonality is continuous across T_m, the magnetic susceptibility is continuous across T_t.

Starting with the premise that the tetragonal phase transition at T_t is induced by the softening of $c_{11}-c_{12}$, we developed a phenomenological model for the temperature dependence of the SDW phase. Between T_t and T_m, this model predicts a new SDW phase, with moments tilted away from the crystal diagonals towards the ab plane.

Returning to the structural phase diagram of Mn-Ni alloys in Fig. 1, we conjecture that the condition $A(T)=A_c$ or $c_{11}^0 - c_{12}^0 + A(T) = 0$ coincides with the thick curve along the tetragonal-to-orthorhombic and cubic-to-tetragonal phase boundaries. Since the tetragonal distortion with $c<a$ is induced by magnetoelastic energies, the elastic constants $\{c_{11}, c_{12}\}$ of this tetragonal phase are identical to the elastic constants $\{c_{11}, c_{12}\}$ of the cubic phase. Hence, the condition $c_{11}-c_{12}=c_{11}^0-c_{12}^0+A(T)>0$ is required for the stability of both the cubic and tetragonal ($c<a$) phases in Fig. 1. Since the thick curve never crosses the Néel temperature, the alloy remains cubic above T_N.

Based on these considerations, we propose the magnetic and structural phase diagram of Fig. 7. It is easy to show that the magnetic transition temperature T_m cannot intersect T_t. Therefore, T_m must intersect the orthorhombic phase boundary below T_t. For Ni concentrations just to the left of the triple point, Fig. 7 permits a series of magnetic phase transitions from S to T to T' to D SDW states.

Similar to MnNi alloys, FeMn alloys also undergo a structural phase transition from cubic to tetragonal. The work of Endoh and Ishikawa[9] on $(Fe_xMn_{1-x})_{0.95}Cu_{0.05}$ alloys has been used to construct the structural phase diagram of Fig. 8. Notice that the Fe-Mn phase diagram contains only two different structural phases, fewer than the four structural phases present in the phase diagram of Mn-Ni alloys. Therefore,

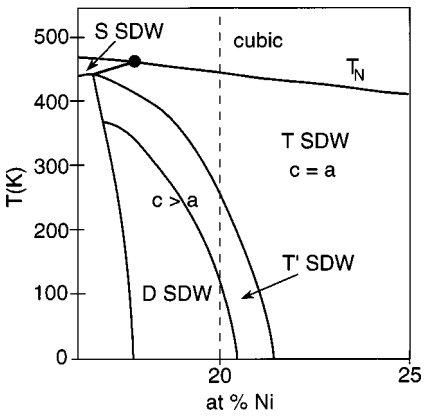

FIG. 7. The proposed magnetic and structural phase diagram of Mn-Ni alloys, indicating the 20% Ni concentration studied in this paper.

Fe-Mn alloys may not permit the same wealth of magnetic behavior as Mn-Ni alloys.

In fact, the magnetic and structural phase transitions in Fe-Mn alloys must coincide. To see this, suppose that the softening of $c_{11}-c_{12}$ is responsible for the cubic-to-tetragonal phase transition in Fe-Mn alloys. Then the condition $A(T)=A_c$ or $c_{11}-c_{12}=0$ would follow the cubic-to-tetragonal phase boundary T_t and continue to hold along the dashed line above T_N in Fig. 8. As a result, Fe-Mn alloys would be tetragonal above T_N to the left of the triple point. Since Fe-Mn alloys are always cubic above T_N, this cannot be the case. Therefore, the T-to-S SDW transition in Fe-Mn alloys should be described by Eq. (14) with $A_c<A(T)$ and $T_m=T_t$. Correspondingly, we do not expect the softening of $c_{11}-c_{12}$ to preceed the cubic-to-tetragonal transition in Fe-Mn alloys.

Recent measurements[30] support these ideas. Resistivity and susceptibility measurements indicate that the structural phase transition in Fe-Mn coincides with the magnetic transition. Unlike in Mn-Ni, the field-cooled and zero field-cooled susceptibilities of Fe-Mn are almost identical for all fields. So there is no sign of hysteretic behavior in Fe-Mn. This substantiates our previous conjecture that the weakly

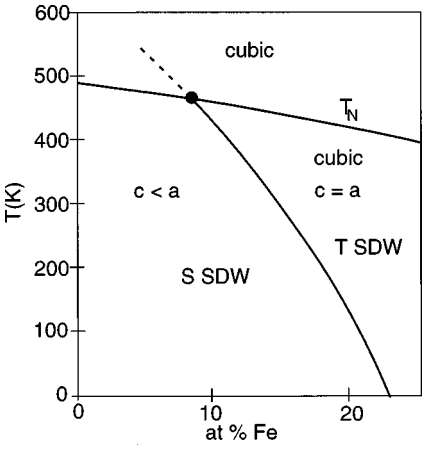

FIG. 8. The magnetic and structural phase diagram of Fe-Mn alloys, based on the work of Ref. 9. If the condition $c_{11}-c_{12}=0$ coincided with the cubic-to-tetragonal phase boundary, then this condition would continue to hold along the dashed line above T_N.

hysteretic behavior in Mn-Ni is due to the freezing of the Ni moments.

As discussed in the previous section, the effective field $\mathbf{B}_i=\zeta\mathbf{M}_i$ must be parallel to the moment $\mathbf{M}_i$ at every site i. The spin-wave (SW) gap $\Delta_{\rm SW}$ evaluated in Ref. 7 was found to be proportional to $\sqrt{\zeta M T_N}$ (the typical SW gap in MnNi and FeMn alloys[31,32] is about 10 meV). Since the magnitude of the effective field $\mathbf{B}_i$ changes at T_m, the SW gap must also change across T_m. To evaluate the relative size of this change, we use Eqs. (7) and (8) to find

$$\zeta^{T'}=-\frac{2V}{3N}s(g_1+3g_2+2g_3M^2), \tag{21}$$

$$\zeta^{D}=-\frac{2V}{3N}\{g_1t+s(g_1+3g_2+3g_3M^2)+6\xi M^2\}. \tag{22}$$

It follows that

$$\frac{(\Delta_{\rm SW}^{T'})^2-(\Delta_{\rm SW}^{D})^2}{(\Delta_{\rm SW}^{T'})^2}=\frac{\zeta^{T'}-\zeta^{D}}{\zeta^{T'}}\sim-\frac{g_3}{g_1+3g_2}M(T_m)^2\geqslant 0, \tag{23}$$

which is a direct measure of the relative size of the quartic magnetoelastic term. If $g_3=0$, then the T' SDW would smoothly evolve into the D SDW, the magnetic susceptibility would be continuous, and the SW gap would show no signs of the magnetic transition. But our susceptibility measurements suggest that the quartic term is nonzero. When $g_3<0$, the SW gap decreases discontinuously below T_m. A similar change in the SW gap is *not* expected in Fe-Mn alloys because the cubic-to-tetragonal transition below T_N has a magnetoelastic origin. Hence, the SW gap of Fe-Mn alloys should be a continuous function of temperature. We hope to test these predictions in the near future.

Several open questions remain. Our proposed form for the noncollinearity energy must be verified through phenomenological or first-principles calculations. There are some indications that the models developed in Ref. 16 and in Sec. III are incomplete. Although Ref. 16 predicted a sharp change in the susceptibility at T_m, the susceptibility plotted in Fig. 6 changes more gradually. This may reveal the coexistence of D and T SDW states over some range of temperatures below T_m.

We are uncertain whether the present model is sufficient to understand the orthorhombic phase of Mn-Ni alloys. It seems likely that the magnetic and structural phase transitions in the orthorhombic phase are also distinct, but this needs to be studied both experimentally and theoretically. Experiments are also required to examine the structural and magnetic phase boundaries of Mn-Ga alloys, which are reported to have a phase diagram similar to that of Mn-Ni alloys.[33]

Obviously, a great deal more experimental work is required to redraw the magnetic phase boundaries of γ-Mn alloys. We hope that the present work provides a roadmap for future exploration of this fascinating system.

ACKNOWLEDGMENTS

This research was supported by Oak Ridge National Laboratory, which is managed by Lockheed Martin Energy Research Corp. for the U.S. Department of Energy under Contract No. DE-AC05-96OR22464.

APPENDIX: ELASTIC CONSTANTS

Above T_t, the elastic energy can be written

$$H_{\rm el}=V\left\{\frac{1}{2}c_{11}(\epsilon_{xx}^2+\epsilon_{yy}^2+\epsilon_{zz}^2)+c_{12}(\epsilon_{xx}\epsilon_{yy}+\epsilon_{yy}\epsilon_{zz}+\epsilon_{zz}\epsilon_{xx})\right\}, \tag{A1}$$

with elastic constants

$$c_{11}=c_{11}^0+\frac{2}{3}A, \tag{A2}$$

$$c_{12}=c_{12}^0-\frac{1}{3}A. \tag{A3}$$

Below T_t, the cubic symmetry is broken and the tetragonal elastic energy must be written

$$H_{\rm el}=V\left\{\frac{1}{2}c_{11}(\epsilon_{xx}^2+\epsilon_{yy}^2)+\frac{1}{2}c_{33}\epsilon_{zz}^2+c_{12}\epsilon_{xx}\epsilon_{yy}+c_{13}(\epsilon_{yy}\epsilon_{zz}+\epsilon_{zz}\epsilon_{xx})\right\}, \tag{A4}$$

with elastic constants

$$c_{11}=\frac{1}{2}(c_{11}^0+c_{12}^0)-\frac{1}{3}A, \tag{A5}$$

$$c_{33}=-c_{11}^0+2c_{12}^0-\frac{4}{3}A, \tag{A6}$$

$$c_{12}=\frac{1}{2}(-c_{11}^0+3c_{12}^0)-\frac{1}{3}A, \tag{A7}$$

$$c_{13}=c_{11}^0+\frac{2}{3}A. \tag{A8}$$

It is important to keep in mind that the strain components in Eq. (A4) are about the new tetragonal structure. So neglecting the magnetoelastic energies, $\epsilon_{ii}=0$ in equilibrium. By contrast, the strain components used in Sec. III, for example, to construct the tetragonality $t=(\epsilon_{xx}+\epsilon_{yy})/2-\epsilon_{zz}$, are deviations from the paramagnetic cubic system. So even in the absence of magnetoelastic energies, $t\neq 0$ for $T<T_t$.

Forgetting about the magnetoelastic energy, the stability of the cubic structure between T_N and T_t requires that $c_{11}-c_{12}=A(T)-A_c>0$ and $c_{11}+2c_{12}=c_{11}^0+2c_{12}^0>0$. Below T_t, the stability of the tetragonal structure requires that $c_{11}-c_{12}=c_{11}^0-c_{12}^0=-A_c>0$ and that the solutions λ to the quadratic equation

$$(c_{11}+c_{12}-\lambda)(c_{33}-\lambda)-2c_{13}^2=0 \tag{A9}$$

are both positive. Using Eqs. (A5)–(A8), these last conditions become $c_{11}^0+2c_{12}^0>0$ and $c_{12}^0-c_{11}^0-A>0$. Hence, $A(T)-A_c$ must be negative below T_t for the tetragonal phase to be stable.

[1] A. Schreyer *et al.*, Europhys. Lett. **32**, 595 (1995); Phys. Rev. Lett. **79**, 4914 (1997).
[2] In a collinear SDW, the moments are parallel to one another. So of the three SDW's in Fig. 1(a), only the *S* SDW is collinear.
[3] D. Meneghetti and S.S. Sidhu, Phys. Rev. **105**, 130 (1957).
[4] T. Jo and K. Hirai, J. Phys. Soc. Jpn. **55**, 2017 (1986).
[5] T. Takahashi, T. Ukai, and N. Mori, J. Appl. Phys. **63**, 3611 (1988).
[6] S. Fujii, S. Ishida, and S. Asano, J. Phys. Soc. Jpn. **60**, 4300 (1991).
[7] R.S. Fishman and S.H. Liu, Phys. Rev. B **59**, 8681 (1999).
[8] J.S. Kouvel and J.S. Kasper, J. Phys. Chem. Solids **24**, 529 (1963).
[9] Y. Endoh and Y. Ishikawa, J. Phys. Soc. Jpn. **30**, 1614 (1971).
[10] H. Uchishiba, J. Phys. Soc. Jpn. **31**, 436 (1971).
[11] N. Honda, Y. Tanji, and Y. Nakagawa, J. Phys. Soc. Jpn. **41**, 1931 (1976).
[12] P. Bisanti, G. Mazzone, and F. Sacchetti, J. Phys. F: Met. Phys. **17**, 1425 (1987).
[13] The locations of the neutron-scattering peaks were used by Uchishiba (Ref. 10) to conclude that the Mn moments in the tetragonal phases with $c/a<1$ and $c/a>1$ lie along the *c* axis and in the *ab* plane, respectively. But this technique cannot distinguish a collinear SDW with moments along the *a* or *b* axis from a noncollinear, *D* SDW.
[14] S.J. Kennedy and T.J. Hicks, J. Phys. F: Met. Phys. **17**, 1599 (1987).
[15] S. Kawarazaki, K. Fujita, K. Yasuda, Y. Sasaki, T. Mizusaki, and A. Hirai, Phys. Rev. Lett. **61**, 471 (1988).
[16] R.S. Fishman and S.H. Liu, Phys. Rev. B **59**, 8672 (1999).
[17] P.A. Fedders and P.C. Martin, Phys. Rev. **143**, 245 (1966).
[18] Reference 7 conjectured that the intensity of incoherent spin excitations would be different in the three SDW states, even when averaged over domains. In particular, these incoherent excitations were not expected in the collinear, *S* SDW state. This conclusion ignored the contribution of the incoherent excitations to the ''silent'' or nonactive satellites of the *S* and *D* SDW states (e.g., the satellites at $\mathbf{Q}_x$ and $\mathbf{Q}_y$ for a *S* SDW with ordering wave vector $\mathbf{Q}_z$). When these silent satellites are included in the average over SDW domains, the intensity of the incoherent excitations (similar to the intensity of the coherent spin-wave excitations) is precisely the same in all three SDW configurations. However, attempts to observe these incoherent excitations in an FeMn alloy have been unsuccessful.
[19] M.W. Long, J. Phys.: Condens. Matter **1**, 2857 (1989).
[20] C.L. Henley, Phys. Rev. Lett. **62**, 2056 (1989).
[21] For an introduction to the neutron scattering techniques, see, for instance, G. E. Bacon, *Neutron Diffraction*, 3rd ed. (Oxford University Press, Oxford, 1975).
[22] See M.J. Cooper and R. Nathans, Acta Crystallogr. **23**, 357 (1967); M. Nielsen and H.B. Möller, Acta Crystallogr., Sect. A: Cryst. Phys., Diffr., Theor. Gen. Crystallogr. **25**, 547 (1969) for methods to calculate the resolution of a triple-axis spectrometer.
[23] Y. Tsunoda and K. Motoya, J. Phys. Soc. Jpn. **62**, 376 (1993).
[24] See, for example, K.H. Fischer and J.A. Hertz, *Spin Glasses* (Cambridge University Press, Cambridge, 1991).
[25] A.P. Ramirez (private communication); Annu. Rev. Mater. Sci. **24**, 453 (1994).
[26] R.A. Cowley, Adv. Phys. **29**, 1 (1980).
[27] R.D. Lowde, R.T. Harley, G.A. Saunders, M. Sato, R. Scherm, and C. Underhill, Proc. R. Soc. London, Ser. A **374**, 87 (1981).
[28] Y. Tsunoda and Y. Nakai, Solid State Commun. **34**, 413 (1980).
[29] Actually, the critical value of *A* is slightly increased by the magnetoelastic energy. Using Eqs. (8) and (10), we find that the shifted critical value is $\tilde{A}_c=A_c+g_1^2/[2(g_3 s+6\xi)]$, slightly greater than A_c.
[30] W.-T. Lee, R.S. Fishman, D. Mandrus, J.L. Robertson, K.J. Song, and J.R. Thompson (unpublished).
[31] Y. Endoh, G. Shirane, Y. Ishikawa, and K. Tajima, Solid State Commun. **13**, 1179 (1973).
[32] K. Mikke, J. Jankowska, and E. Jaworska, Physica B **120**, 156 (1983).
[33] T. Hori, Y. Morii, S. Funahashi, H. Niida, M. Akimitsu, and Y. Nakagawa, Physica B **213&214**, 354 (1995). .